RSC Advances

PAPER

View Article Online
View Journal | View Issue



Cite this: *RSC Adv.*, 2022, **12**, 12564

# Unveiling of a smartphone-mediated ratiometric chemosensor towards the nanomolar level detection of lethal $CN^-$: combined experimental and theoretical validation with the proposition of a molecular logic circuitry†

Suparna Paul, [ab] Udayan Mondal, [ab] Somrita Nag,[ab] Madhupa Seth[c] and Priyabrata Banerjee *[ab]

A promising naphthalene-functionalized ratiometric chemosensor (*E*)-1-((naphthalen-5-yl) methylene)-2-(2,4-dinitrophenyl) hydrazine (**DNMH**) is unveiled in the present work. **DNMH** demonstrates brisk discernible colorimetric response from yellow to red in the presence of $CN^-$, a lethal environmental contaminant, in a near-perfect aqueous medium with a LOD of 278 nM. The "key role marker" controlling the electrochemical and non-covalent H-bonding interaction between **DNMH** and $CN^-$ is through the commendable role of acidic –NH functionalities. Kinetic studies reveal a pseudo second order reaction rate and the formation of an unprecedented photostable adduct. The negative value of $\Delta G$ as evaluated from ITC substantiates the spontaneity of the **DNMH**$\cdots CN^-$ interaction. The sensing mechanism was further reinforced with state-of-the-art theoretical investigations, namely DFT, TDDFT and Fukui indices (FIs). Moreover, the proposition of a reversible multi-component logic circuitry implementing Boolean functions in molecular electronics has also been triggered by the turn-over spectrophotometric response of the ditopic ions $CN^-$ and $Cd^{2+}$. The cytotoxicity of **DNMH** towards *Bacillus thuringiensis* and *Escherichia coli* is successfully investigated *via* the MTT assay. Impressively, "dip stick" and "easy to prepare" test paper device and silica gel-based solid-phase $CN^-$ recognition validate the on-site analytical application of **DNMH**. Furthermore, the involvement of a synergistic approach between '*chemistry beyond the molecule*' and 'engineering' *via* an exquisitely implemented smartphone-assisted colorimetric sensory prototype makes this work unprecedented among its congeners and introduces a new frontier in multitudinous material-based functional product development.

Received 24th September 2021
Accepted 31st March 2022

DOI: 10.1039/d1ra07139d

rsc.li/rsc-advances



## Introduction

In the 21st century, the state-of-the-art flourishing advancements in mobile information and communication technologies by the conversion of lab-scale data to electronic data and their subsequent synchronization with the Internet of Things (IoT) technology have attracted significant attention from researchers. In this regard, smartphones with user-friendly applications have facilitated as well as brought about a new frontier in the multifaceted functional material-based world of recognition and digitalization.[1,2] As a consequence, smartphone-affixed sensory devices serve as an emerging analytical platform for formulating cost-effective and versatile "all-in-one" sensing systems by simplifying the design of sophisticated instrumental devices. This technology also offers instantaneous and brisk quantification of targeted guest analytes. The harmonization of a designed chemical sensor in combination with the computational power of a smartphone in an efficient manner provides precise acquisition of data regarding targeted analyte recognition. Thus, it expands real-world viability in resource-constrained regions where sophisticated spectroscopic analytical and monitoring technologies are inaccessible.[3] Therefore, in the present work, by taking advantage of the imaging module, a smartphone-assisted colorimetric

[a]*Surface Engineering & Tribology Group, CSIR-Central Mechanical Engineering Research Institute, M. G. Avenue, Durgapur-713209, India. E-mail: pr_banerjee@cmeri.res.in; https://www.cmeri.res.in; https://www.priyabratabanerjee.in*

[b]*Academy of Scientific & Innovative Research (AcSIR), Ghaziabad-201002, Uttar Pradesh, India*

[c]*Department of Microbiology, The University of Burdwan, Burdwan-713104, West Bengal, India*

† Electronic supplementary information (ESI) available: Experimental details of **DNMH** *i.e.*, its ESI-MS, $^1$H-NMR, Crystallographic data for CCDC No 2019887, solvatochromism, B–H plot, LOD, electrochemical response, Logic Gate, DLS, FT-IR, details of MTT Assay, DFT. TDDFT and FIs calculation details [coordinates used for **DNMH** have been provided], Plausible mechanism, AutoCAD diagram @ Smartphone prototype. CCDC 2019887. For ESI and crystallographic data in CIF or other electronic format see **https://doi.org/10.1039/d1ra07139d**

prototype has been successfully integrated with an indigenously developed optical chemosensor for the synchronous "color to concentration" detection cum quantification of $CN^-$ like environmental pollutant in a near-perfect aqueous medium.

The selective recognition of environmentally and biologically significant anions[4–7] such as $CN^-$ has lured immense research interest owing to their ubiquitous nature.[8–10] Despite its daunting toxicity, this chemical warfare agent is utilized in various industrial processes.[11–13] Consequently, indiscriminate utilization in several industries along with its natural release from various plants, bacteria, algae, and fungal species, where it behaves as a secondary metabolite, are responsible for the threat of $CN^-$ poisoning.[14]

As a consequence, there arises an exigency to develop reliable, less cumbersome synthetic strategies and inexpensive and rapid "naked-eye-responsive" smart molecular probes for the discernible detection of $CN^-$ (below the explicitly stipulated standards of $CN^-$ in drinking water, *i.e.*, 1.9 μM as per W.H.O guidelines).[15] There are a few traditional techniques available for $CN^-$ detection, including electrochemistry, polarography, potentiometry, flow injection amperometry and ion chromatography.[16–18] However, complicated sample pre-treatment, delayed detection, expensive bulky instrumentation, reduced portability, lack of real-time analysis, perturbation from competitive species, and the requirement of skilled manpower often hinder these existing methodologies from real-world application.

In this context, "ratiometric optical sensors" are exquisitely appealing owing to their simplicity, high sensitivity, ease of real-time monitoring, internal calibration effect to minimize interference from deviations of local sensor concentration and microenvironment,[19] anti-interference ability and rapid "naked eye" visualization with a low detection threshold. Furthermore, assessment of the ratio of spectroscopic behavior obtained at two varying wavelengths allows for the preferential selection of ratiometric probes over the conventional techniques of absorbance measurement at a definite wavelength.[20] Most importantly, integration of the chemical output obtained from solution-state sensing with fabricated RGB-based smartphone devices provides an exquisite platform for the coherent recognition of $CN^-$ that overcomes the major limitations of the current methodologies.[21–24]

Therefore, as part of our longstanding research endeavor in the supramolecular domain,[25–35] we aimed to thoughtfully design a naphthalene–hydrazine decorated Schiff base organic compound (SOC). Herein, functionalization of the anion recognition site (–NH) with a dinitrophenyl-like chromophore moiety extends the overall π-conjugation within the molecular scaffold. This is realized in the promising "naked eye" colorimetric change from yellow to red towards selective detection of $CN^-$ in a near-perfect aqueous medium with favorable sensitivity and accuracy. The presence of a nitro substituent also amplifies the acidity of –NH functionalities, thereby enhancing the affinity of the molecular recognition event by supramolecular hydrogen bonding interaction between **DNMH** and $CN^-$. The novelty of the present work lies in the synergistic approach between 'chemistry beyond the molecule' and 'engineering' *via* a suitably implemented smartphone-based colorimetric sensory prototype towards the real-time monitoring of $CN^-$, which to the best of our knowledge is still scantily explored in the supramolecular realm.

## Experimental

### Materials and instrumentation

The required synthons and solvents are commercially available and were used as obtained. All the $TBA^+X^-$ salts including cyanide, fluoride, chloride, acetate, bromide, nitrates, and carbonates were procured from Sigma Aldrich and iodide and sulphates were purchased from Alfa Aesar. Spectroscopic-grade solvents like acetonitrile, dimethyl sulfoxide and water have been obtained from Merck (India) Pvt. Ltd.

**DNMH** has been structurally confirmed by mass spectrometry (Advion Make; Serial no. 3013-0140) and $^1$H-NMR spectroscopy (Bruker 400 MHz NMR spectrometer). The functional groups within the **DNMH** scaffold have been authenticated by FT-IR spectroscopy (Spectrum 65, PerkinElmer). X-ray crystallography was performed in a Bruker D8 Venture (APEX-III) diffractometer equipped with a photon detector and assisted by graphite-monochromated Mo Kα ($\lambda = 0.71073$ Å) irradiation. A CARY60 spectrophotometer was used to perform the UV-vis spectrophotometric study. Particle size analysis of **DNMH** and the **DNMH** + $CN^-$ adduct was executed by a dynamic light scattering study (Zetasizer Nano ZS90). Cyclic voltammetry was performed in a CH instrument.

### Computational method

Density functional theory calculations have been performed using the Turbomole (V7.0) software (TmoleX interface, 4.1.1) to gain deep insight into the plausible mechanistic pathway of the host–guest interaction. (B3LYP)/def SV(P) are the basis sets used during the ground-state geometry optimizations. For atoms like nitrogen, oxygen, carbon and hydrogen, the basis set of def-SV(P) was used. Material studio TM (version 6.1) possessing the DMol3 module was used to calculate the Fukui indices of the respective systems.[36] Double numerical basis set plus polarization (DNP) atomic orbital in line with generalized gradient approximation (GGA) and the Becke, 3-parameter, Lee–Yang–Parr (B3LYP) exchange correlation hybrid functional were used for calculating the FIs.

### Synthetic procedure of the chemosensor DNMH

**DNMH** was successfully synthesized *via* the one-pot condensation of 1-naphthaldehyde (1 mmol, 156.18 mg) and 2,4-dinitrophenylhydrazine (1 mmol, 198.14 mg) in methanol with continuous stirring for 5 hours under ambient conditions (Scheme 1). The mustard yellow colored product so obtained was purified by washing with methanol and finally collected after drying in vacuum to obtain the desired compound (*E*)-1-((naphthalen-5-yl) methylene)-2-(2,4-dinitrophenyl) hydrazine (henceforth abbreviated as **DNMH**).

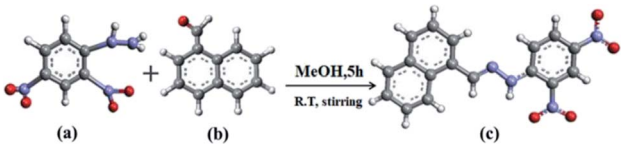


Scheme 1 Structural representation of (a) 2.4-dinitrophenyl hydrazine, (b) 1-naphthaldehyde and the final product (c) (*E*)-1-((naphthalen-5-yl) methylene)-2-(2,4-dinitrophenyl) hydrazine (**DNMH**).

## Results and discussion

**DNMH** was characterized by ESI-MS, $^1$H-NMR and solid-state elemental analyses such as SCXRD and FT-IR. Yield: 80%, ESI-MS (+) mode: *m*/*z* calculated = 336.3 (**DNMH**), found 359.3 (**DNMH** + $Na^+$) 375.1 (**DNMH** + $K^+$), $^1$H-NMR (400 MHz, ACN-$d_3$, $Me_4Si$); $\delta$ = 11.8 (s, $^1$H, amine), 9.5 (s, $^1$H, imine) (Fig. S1 and S2†).

### X-ray crystallography

The as-synthesized product was layered with tetrahydrofuran : hexane (1 : 1, v/v) to obtain needle-shaped crystals of the desired compound **DNMH**. The molecule crystallizes in the *P*21/*n* space group. Two molecules of **DNMH** are present within the unit cell crystallographic axis, wherein a centrosymmetric oriented structure is observed (Fig. 1a). The aromatic rings of two **DNMH** molecules are 3.7 Å apart, indicating an extensive π–π stacking interaction (face to face or sandwich) (Fig. 1b), which certainly provides additional stability to the chemosensor.

**DNMH** possesses an *i*-centre since the naphthalene unit of one molecule and the benzene of the other are aligned in a trans manner to avoid electronic repulsion between the $-NO_2$ groups of each **DNMH** molecule. According to Zimmerman's molecular tweezers model, the fused aromatic rings are considered to be two tweezers where the stacking interactions are associated with minimal π overlap.[37] The open cavities of these molecular tweezers accelerate the binding of guest $CN^-$ *via* hydrogen bonding interaction with the –NH proton of **DNMH**. The ORTEP with 50% probability is displayed in Fig. 1c. The aldimine (–CH=N–) bond length is observed to be 1.30 Å, which is in accordance with the literature (1.27 Å). This slight deviation from the ideal bond distance implies sufficient delocalization of electron density within the π-conjugated system, *i.e.*, the five (phenyl) and six-membered ring (naphthalene) structure of naphthalene and phenyl hydrazine moieties as well as due to the presence of the $-NO_2$ substituent within **DNMH**. In the hydrazine unit, the N–N bond distance is observed to be 1.38 Å, slightly reduced compared to that of unsubstituted hydrazine (1.45 Å). This deviation may be attributed to the strong π-conjugation effect localized at the N–N terminal bond length due to the conjugation of the lone pair of electrons on the N atom (amine) with the π electrons in the molecule. As a result, the N–N bond distance is shortened, which causes an increase in the azomethine (C=N) bond length. The N–H bond distance is found to be 1.03 Å. The bond angle between N(005)-N(007)–C(00H) is 115.67°, whilst the N(007)–C(00H)–C(00F) angle is 119.09°. Although C(00H) and N(007) denote $sp^2$ hybridized atoms, their slight deviation from the ideal $sp^2$ hybridized bond angle (120°) suggests repulsion between the lone pair of electrons localized on the N atoms and its adjacent bonds causing an appreciable strenuous environment within the system. There is extensive intramolecular H-bonding between the O atom of $-NO_2$ and –NH proton of the aldimine unit in **DNMH**, as well as intermolecular H-bonding of one **DNMH** with the other identical molecule that further causes stabilization of the system (Fig. S3†). The packing arrangement of **DNMH** in a unit cell (Fig. S4†) along with the detailed crystallographic information and bond parameters of **DNMH** are tabulated in Table S1–S5†.

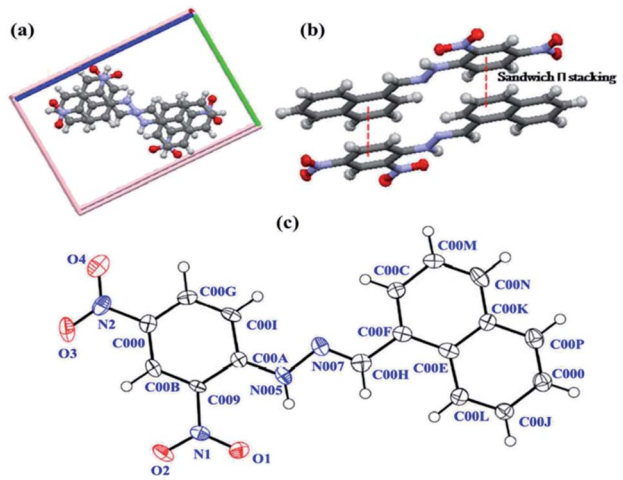


Fig. 1 (a) Closely packed centrosymmetric oriented confirmation of DNMH; (b) face to face π interaction; (c) ORTEP of DNMH with atom numbering (50% probability).

**"Naked eye" visualization of DNMH in the presence of $CN^-$ and various other anions.**

**DNMH** displayed solvatochromic behavior, owing to which the electronic spectra of **DNMH** have been recorded in a series of solvents of varying polarity, namely acetonitrile, dichloromethane, hexane, methanol, tetrahydrofuran, dimethyl sulfoxide, toluene, xylene, benzene, chloroform, dioxane, ethanol, isopropanol and water (Fig. S5†). Thereafter, the spectroscopic analysis of **DNMH** ($1 \times 10^{-5}$ M) in a DMSO/ACN mixture (1 : 9 v/v) in the presence of different anions was performed. Interestingly, a distinct yellow to red color change was observed only in the presence of $CN^-$ ($1 \times 10^{-4}$ M) in a near-perfect ACN/water mixture (4 : 1 v/v, Fig. 2a). However, no other anions offered any substantial change in the yellow color of the **DNMH** solution. In addition, the colorimetric response and optical performance of the chemoreceptor **DNMH** with $CN^-$ have been investigated in an organo-aqueous mixture of varying stoichiometry to validate the best solvent mixture ratio wherein the chromogenic detection of $CN^-$ is the most promising (Fig. S6 and S7†).

The translation in the optical properties of **DNMH** in the presence of $CN^-$ was probed by UV-vis spectroscopic analysis. **DNMH** exhibited two absorption bands at 315 nm and 390 nm ($\lambda_{max}$/nm; $\varepsilon/M^{-1}$ $cm^{-1}$: 26 800) (Fig. S8†). The former band corresponds to the electronic transition from (S0 → S1), *i.e.*, π–

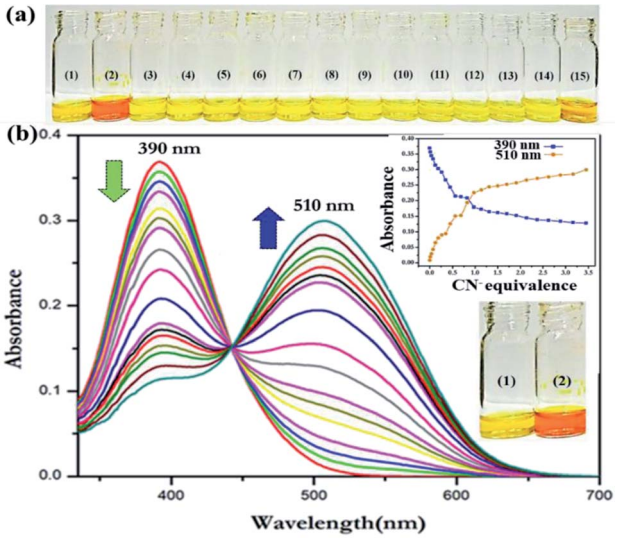


Fig. 2 (a) Naked eye colorimetric changes of **DNMH** ($1 \times 10^{-5}$ M, ACN) in the presence of various anions ($1 \times 10^{-4}$ M) in the ACN/$H_2O$ mixture (4 : 1 v/v): 1. **DNMH**, 2. **DNMH** + $CN^-$, 3. **DNMH** + $Cl^-$, 4. **DNMH** + $SO_4^{2-}$, 5. **DNMH** + $OAc^-$, 6. **DNMH** + $NO^{3-}$, 7. **DNMH** + $CO_3^{2-}$, 8. **DNMH** + $I^-$, 9. **DNMH** + $Br^-$, 10. **DNMH** + $PO_4^{3-}$, 11. **DNMH** + $ClO_4^-$, 12. **DNMH** + $MnO_4^-$, 13. **DNMH** + $AsO_2^-$, 14. **DNMH** + $AsO_4^{3-}$, and 15. **DNMH** + $F^-$; (b) UV-vis titration of **DNMH** ($1 \times 10^{-5}$ M) in $CH_3CN$ with sequential addition of $CN^-$ ($1 \times 10^{-4}$ M) (ACN : $H_2O$ = 4 : 1 v/v) [inset: ratiometric plot of **DNMH** with $CN^-$ at 390 nm and 510 nm and vials containing (1) **DNMH** and (2) **DNMH** + $CN^-$ solution].

π* transition, which does not get altered in varying solvents; however, the type and positions of the substituents that are located on the phenyl rings make it sensitive. The latter one is due to the n–π* transition that occurs owing to the lone pair of electrons of the nitrogen atom being promoted to the π* orbital of the –CH=N– group. Intramolecular charge transfer (ICT) from the azomethine center to the electron-withdrawing $-NO_2$ groups is also responsible for the latter band. When $CN^-$ ($1 \times 10^{-4}$ M) was added to the **DNMH** ($1 \times 10^{-5}$ M) solution, the 390 nm peak progressively decreased with concomitant generation of a new peak at 510 nm ($\lambda_{max}$/nm; $\varepsilon/M^{-1}$ $cm^{-1}$: 30 100) (Fig. 2b), implicating the recognition event to be ratiometric in nature. The appearance of the 510 nm peak authenticates the **DNMH**···$CN^-$ adduct formation and the considerable bathochromic shift in ICT is also in accordance with the extensive H-bonding interaction between the –NH and –CH protons of **DNMH** with the target $CN^-$. Due to this non-covalent interaction, a $\delta^-$ charge is generated on the N atom and is subsequently delocalized in the DNP unit (acceptor) of **DNMH**. This activates the ICT process and the drastic color change from yellow to red. The appearance of the isosbestic point at 440 nm and variation of spectral intensity with increasing $CN^-$ amount indicate a good host–guest binding interaction. The Job plot method of continuous variation validates the 1 : 1-type binding stoichiometry between **DNMH** and $CN^-$ (Fig. S9†). From the B–H plot, the association constant ($K_a$) was evaluated to be $4.48 \times 10^6$ $M^{-1}$, which further confirms a strong binding interaction (Fig. S10†). The detection threshold of $CN^-$ by **DNMH** has been observed to be 278 nM (Fig. S11†), which is lower than the MCL value of $CN^-$ (1.9 μM) as per the W.H.O. guidelines. **DNMH**···$CN^-$ exhibits a swift sensing response (~8 seconds) (Fig. S12†) and an unprecedented photo stability that provides an additional advantage for long-duration monitoring applications (Fig. S13†).

## Electrochemical studies

Electrochemical analysis of **DNMH** displayed a cathodic peak at −0.66 V (current height 0.0086 mA) and a weak anodic peak at 0.50 V (current height −0.00138 mA) (Fig. S14†). Upon gradual addition of $CN^-$ ($10^{-3}$ M, ACN : $H_2O$, 4 : 1 v/v) in the **DNMH** solution, the cathodic peak was steadily diminished (Fig. S15†). From this, it could be speculated that upon interaction of $CN^-$ with the –NH proton of **DNMH**, the N atom of **DNMH** acquired partial negative charge. This caused an enhancement in the electron density of the overall system. The reduction process in turn was restricted, which reduced the cathodic peak potential and facilitated the oxidation of the system by enhancing the anodic peak potential. The redox potential of **DNMH** with $CN^-$ has been tabulated (Table S6†).

## Isothermal titration calorimetry (ITC)

ITC analysis has been performed to obtain deeper insight in determining the thermodynamic parameters, *i.e.*, the enthalpy change ($\Delta H$), entropy change ($\Delta S$), Gibbs free energy change ($\Delta G$), association constant ($K$) and the number of binding sites ($n$) involved in the host (**DNMH**) and guest ($CN^-$) interaction. ITC was performed at 25 °C using the simple injection methodology.[38] The evolution of heat per mole of $CN^-$ plotted against the molar ratio of **DNMH** is clearly depicted in Fig. S16.† Herein, the number of binding sites ($n$) was evaluated to be 0.685 ± 0.0279. The enthalpy and entropy changes were calculated to be $3.613 \times 10^6 \pm 2.745 \times 10^5$ cal $mol^{-1}$ ($15.1746 \pm 2.745 \times 10^5 \times 10^6$ J $mol^{-1}$) and $1.22 \times 10^4$ cal $mol^{-1}$ $deg^{-1}$ ($5.124 \times 10^4$ J $mol^{-1}$ $deg^{-1}$), respectively, having a $K_a$ of $1.02 \pm 7.53 \times 10^8 \times 10^9$. Besides, from the Gibbs equation ($\Delta G = \Delta H - T\Delta S$), $\Delta G$ was deduced to be −94.92 J $mol^{-1}$, which substantiates the spontaneity of the interaction between **DNMH** and $CN^-$.

## Proposition of a logic gate-based ensemble

The [**DNMH**···$CN^-$] ensemble was utilized to investigate its reversibility in the presence of various cations. Interestingly, it was observed that the reddish orange color of the ensemble changed to light yellow in the presence of only $Cd^{2+}$, whereas for the other cations, the color of the adduct solution remained unperturbed (Fig. S17†). This indicated the profound selective nature of the ensemble towards $Cd^{2+}$ only. Such restoration of color not only implies that the process of interaction is reversible but also strengthens the presence of H-bonding between **DNMH**···$CN^-$ (Fig. 3a). This reversibility of **DNMH** has instigated the proposition of the multi-component supramolecular gate function and arithmetic calculation.[39] Therefore, molecular level combinational AND–NOT logic circuits have been established using **DNMH**, $CN^-$ and $Cd^{2+}$.

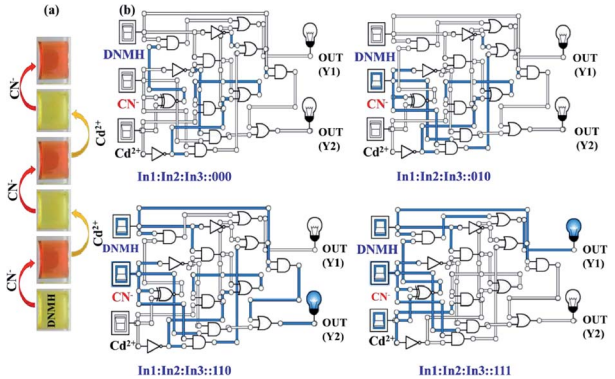


Fig. 3 (a) Sequential colorimetric reversibility of **DNMH** with alternate addition of $CN^-$ ($1 \times 10^{-4}$ M, ACN : $H_2O$ = 4 : 1 v/v) and $Cd^{2+}$ ($1 \times 10^{-4}$ M, $H_2O$); (b) proposition of a molecular logic gate by various AND–NOT–XNOR–NAND–OR logic functions as inputs.

The UV-vis spectral data of **DNMH** ($10^{-5}$ M) in the presence of $CN^-$ ($10^{-4}$ M) resulted in an output value at 510 nm. Here, we get an AND logic circuit by considering the two input (In) system, in which In 1: **DNMH** and In 2: $CN^-$. The output will be high if the input is high and the output will be ON if both the inputs In 1 and In 2 are on or else the output will be OFF. Another three-input combinational circuit was developed: In 1: **DNMH**, In 2: $CN^-$, and In 3: $Cd^{2+}$. **DNMH** in the presence of $CN^-$ afforded UV-vis spectral response (In: ON) at 510 nm, which was diminished in the presence of $Cd^{2+}$ and we get the output OFF at 510 nm. The repetition of OFF/ON was observed for **DNMH** with alternate $CN^-$ and $Cd^{2+}$ addition. Finally, the AND–NOT–XNOR–NAND–OR logic functions were obtained by considering the three combinational input circuits (Fig. 3b and S18†). The spectrophotometric analysis of **DNMH** with $CN^-$ and $Cd^{2+}$ is presented in the truth table (Table S7†).

### $^1$H-NMR titration of DNMH with $CN^-$

$^1$H-NMR spectroscopy provides deep insight into the structural properties of **DNMH** as well as the probable binding mode of **DNMH** and $CN^-$. Herein, the chemical shifts around $\delta$ = 11.8 ppm and $\delta$ = 9.5 ppm correspond to the secondary amine (–NH) proton and imine (–CH=N–) protons. Steady addition of $CN^-$ to **DNMH** solution causes the –NH proton peak to gradually diminish with continuous up-field shifting due to the strong intermolecular –NH–$NC^-$ hydrogen bonding interaction. In addition, the presence of $CN^-$ causes an up-field shift of the –NH proton that falls within the shielding zone of the ring current of the triple bond in the $CN^-$ ion.[40] The aldimine proton peak was also diminished weakly and slightly shielded upon interaction with $CN^-$. The other skeletal proton signals were shifted up-field on coordinating with $CN^-$ due to the delocalization of the negative charge on the –NH and –CH center throughout the **DNMH** molecule. Moreover, the absence of any new peak around $\delta$ = 5–6 ppm ruled out the possibilities of deprotonation of the –NH proton or nucleophilic addition to the imine center, thereby strengthening the intermolecular H-bonding interaction between –NH···$NC^-$ (Fig. 4). In addition, the particle size distribution and FT-IR analysis of **DNMH** and

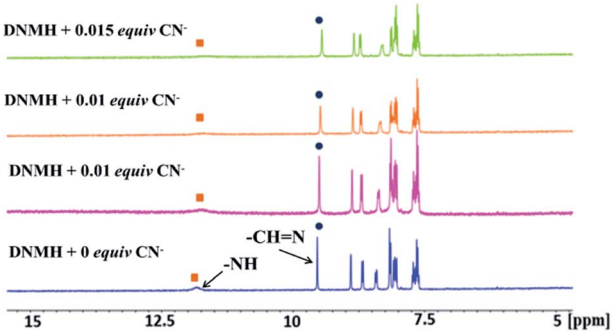


Fig. 4 $^1$H-NMR titration spectra of **DNMH** with $CN^-$ in ACN-$d_3$.

the **DNMH**···$CN^-$ adduct also show similar results (Fig. S19 and S20†).

### Antibacterial assay

To examine the effect of varying **DNMH** concentration on the Gram-positive bacterium *Bacillus thuringiensis* (*Bt*) and the Gram-negative bacterium *Escherichia coli* (*E. coli*), cytotoxicity assays (MTT) were performed. Cytotoxicity study revealed optimal activity at $10^{-7}$ M concentration, and $10^{-2}$ M was found to be the minimal inhibitory concentration (cytotoxic concentration), *i.e.*, with increasing **DNMH** concentration, the viability of *Bt* and *E. coli* cells gradually reduced. The comparative cytotoxicity analysis with varying concentration ($10^{-2}$ to $10^{-7}$ M) displayed that around 60% of *Bt* cells and 50% of *E. coli* cells (Fig. 5) remained alive in a concentration of **DNMH** of $10^{-7}$ M.

### An in-depth theoretical insight by TDDFT and DFT

To congregate the detailed information regarding the experimentally obtained absorption bands of **DNMH** and **DNMH**···$CN^-$, TDDFT calculations were performed. The B3LYP hybrid functional and defSV(P)/defTZVP basis sets were used in the Turbomole (V7.0) software TmoleX interface, 4.1.1.[41] The experimental and simulated spectra (applying COSMO/acetonitrile) of **DNMH** and **DNMH**···$CN^-$ are shown in Fig. S21†. In the case of **DNMH**, the simulated peak at 425 nm is in good agreement with the experimentally obtained $\lambda_{max}$ at 390 nm. For the **DNMH**···$CN^-$ adduct, the theoretical peak at

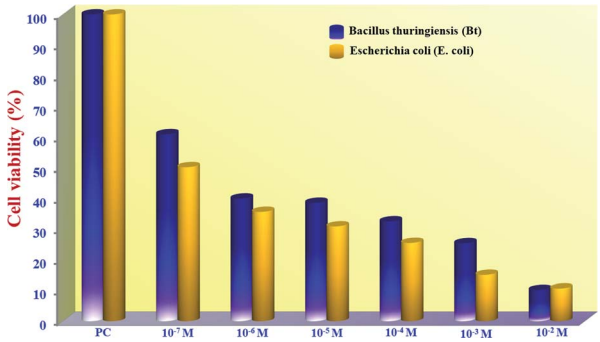


Fig. 5 MTT assay of *Bacillus thuringiensis* (Gram-positive bacterium) and *E. coli* (Gram-negative bacterium) treated in the presence of **DNMH** incubated at 37 °C.

550 nm appeared close to its experimentally resolved $\lambda_{max}$ at 510 nm. The major electronic excitation calculations and coordinates for the TDDFT of **DNMH** and **DNMH**$\cdots CN^-$ are presented in Table S8–S10†.

To the optimized geometry of **DNMH**, $NMe_4CN$ was added and a geometry optimized structure of the **DNMH**/$CN^-$ (1 : 1) complex was obtained. The N–H bond length of the optimized **DNMH** structure was found to increase from 1.025 Å to 1.046 Å owing to facile hydrogen bonding interaction between the –NH and –CH hydrogen of **DNMH** with $CN^-$. The plausible interaction of **D NMH** with $CN^-$ is depicted in Fig. S22†. The host and guest binding interaction may be attributed to the strong hydrogen bonding interaction of **DNMH** with $CN^-$. In this regard, when the electron-rich naphthalene donor within the molecular scaffold of **DNMH** interacts with the guest analyte $CN^-$, the electron-withdrawing ability of the acceptor ($CN^-$) is strengthened and consequently the $\Delta E$ of the host (**DNMH**) and host–guest adduct (**DNMH**$\cdots CN^-$) are significantly reduced from 2.972 eV to 1.729 eV.[42] This is also in good agreement with the bathochromic shift ($\Delta\lambda$ = 120 nm) in the UV absorption wavelength of **DNMH** from 390 nm to 510 nm upon analyte recognition. The overall energy of the **DNMH**$\cdots CN^-$ adduct was observed to be −1480.941 Hartree, which is certainly more stabilized than the sole chemosensor **DNMH** (−1173.22 Hartree). The geometry optimized structure of **DNMH** suggested that the naphthalene moiety acts as the HOMO and 2,4-dinitro phenyl hydrazine as the LUMO owing to their electron density difference (Fig. S23a and b†). However, upon interaction with $CN^-$, the electron density and energy of the HOMO decreased, resulting in reduction of $\Delta E$ (Fig. S23c, d and Table S12†). In the $^1$H-NMR spectra as well, the peak of the –NH proton was diminished and slightly up-field shifted upon gradual addition of $CN^-$ due to the hydrogen bonding interaction. There is no experimental and theoretical proof for the deprotonation of the –NH proton. Thus, the performed theoretical calculation is in good corroboration with the experimental findings. Fig. 6 displays the overall energy and HOMO–LUMO bad gap of **DNMH** and the **DNMH**$\cdots CN^-$ adduct.

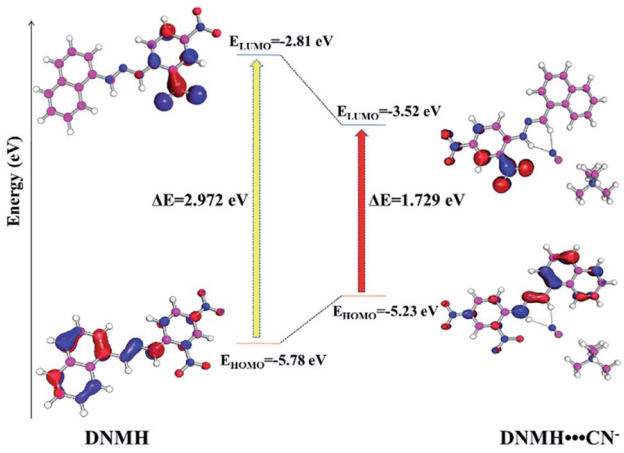


Fig. 6 HOMO–LUMO band gap and geometry optimized structures of DNMH and the DNMH$\cdots CN^-$ adduct.

## Fukui index analysis

Fukui index (FI) or reactivity index analysis provides detailed information (based on electron density) about the active sites or donor centers present within a chemosensor molecule, *i.e.*, the underlying host–guest interaction may be convincingly understood.[43]

While determining the $f_k^+$ of the active sites, it was observed that the calculated Mulliken and Hirshfeld electron density values localized on the plausible donor centers in the **DNMH** molecules are N5: 0.019, 0.025; N7: −0.001, 0.008; C17: 0.029, 0.026; H26: 0.017, 0.014; and H30: 0.014, 0.009. For **DNMH**$\cdots CN^-$, N5: 0.019, 0.023; N7: −0.000, 0.008; C17: 0.031, 0.027; H33: 0.009, 0.008; and H37: 0.012, 0.007. Hence, for $f_k^+$ analysis, the change in electron distribution in the donor centers before and after interaction with $CN^-$ is very less. Then, the FI for $f_k^-$ was also determined. In this case, the calculated Mulliken and Hirshfeld electron density values localized on the plausible donor centers in the **DNMH** molecules were found to be N5: 0.038, 0.043; N7: −0.046, 0.05; C17: 0.027, 0.030; H26: 0.019, 0.015; and H30: 0.029, 0.017. For **DNMH**$\cdots CN^-$, N5: 0.047, 0.051; N7: 0.053, 0.055; C17: 0.035, 0.036; H33: 0.016, 0.013; and H37: 0.025, 0.014. The $f_k^-$ values clearly depict that the donor centers (N5, N7 and C17) became electron-rich after undergoing H-bonding interaction with $CN^-$. Therefore, the electron density on the H atoms (H26 and H30 in **DNMH**) as expected was considerably reduced after analyte interaction (H33 and H37 in **DNMH**$\cdots CN^-$). The isosurface plots corresponding to $f_k^+$ and $f_k^-$ attack for **DNMH** and **DNMH**$\cdots CN^-$ have been acquired from the Dmol$^3$ module with an isovalue of 0.01 (Fig. 7). The coordinates for the Fukui analysis are tabulated in Table S13–S16†.

## Sensing potential towards $CN^-$ of the test paper device and silica gel-based assay: practical application

Detection of $CN^-$ by virtue of the "dip stick"-based sensing platform is considered to be a promising alternative to laboratory-based instruments owing to several advantages, such as simplicity, portability, cost effectiveness and disposability.[44] Herein, chromatographic strips were utilized as a solid support

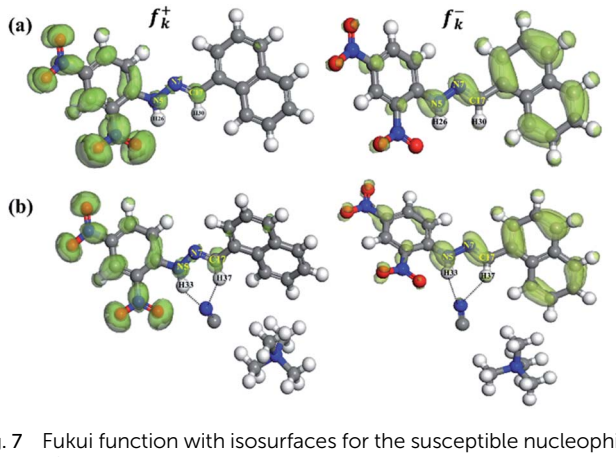


Fig. 7 Fukui function with isosurfaces for the susceptible nucleophilic attack ($f_k^+$) and electrophilic attack ($f_k^-$) of (a) DNMH and (b) DNMH$\cdots CN^-$ from the DMol3 module possessing an isovalue of 0.01.

towards the facile impregnation of **DNMH** ($10^{-3}$ M, $CH_3CN$). The test paper strips were then dried and $CN^-$ solution was dropped on the surface of the strip using a capillary tube. Immediately, the color changed from bright yellow to an intense red, as shown in Fig. 8a. The appearance of red coloration strengthens the potentiality of **DNMH** as a tool for lethal $CN^-$ detection in analytical and environmental applications while eliminating the need for sophisticated equipment or well-controlled environments.

Thereafter, silica gel-based assay was also instigated for investigating the fate of $CN^-$ detection by **DNMH** in a solid medium.[45] Initially 1 g silica gel of 60–120 mesh size was immersed in **DNMH** ($CH_3CN$ solution, 5 mL $1 \times 10^{-3}$ M) and the solvent was removed. A faint yellow coloration was imparted to the silica. The silica gel-loaded **DNMH** was further treated with a 5 mL solution of $CN^-$ [$1 \times 10^{-2}$ M, $CH_3CN : H_2O = 4 : 1$ v/v]. An intense color change from faint yellow to red was observed immediately (Fig. 8b). The solvent was then removed under reduced pressure and the so-obtained red colored silica powder was dried in an oven. This indicates that **DNMH** could be successfully employed for solid-state $CN^-$ detection as well.

## Smartphone-assisted colorimetric sensory prototype for onsite $CN^-$ detection

Till date, various conventional techniques including titrimetric, voltammetric, potentiometric, and electrochemical methods have been explored towards $CN^-$ detection. However, these techniques are relatively cumbersome, involve bulky laboratory instruments, tedious sample pre-treatment, and a lack of user affability, and require long detection periods. These altogether have greatly limited their practical applicability. In this regard, chromogenic assays provide a straightforward and facile way of precise monitoring of the presence of targeted guest analytes. Moreover, smartphone-assisted colorimetric assays further miniaturize the chromogenic sensing system by providing a portable, affordable and convenient platform to recognize specific target analytes. Herein, digitalization of the chromogenic colorimetric outcome of **DNMH** has been rendered into RGB-based digital outputs, embedded with the wireless communication technology 1Sheeld.[46] The 1Sheeld turns the smartphone into different Arduino shields and finally an economic, easy to operate and layman's sensory prototype was obtained for the on-field recognition of $CN^-$. This certainly makes the present work unprecedented among its congeners and hitherto less explored. The overview and segment-wise visualization of the fabricated smartphone-assisted sensory prototype along with its AutoCAD diagram (SOLIDWORKS Software) are provided in Fig. S24–S29†.

## Working principle of the prototype

At the outset, the vial containing the chemosensor **(DNMH)** solution (control) is to be mounted on the sample holder and the lid is covered from the top. The flashlight or torch of the smartphone is turned on since there is no light inside the black acrylic prototype box, and here the camera of the smartphone acts as the color detector/sensor. It can capture images of the sample solution (**DNMH**: yellow color) in the vial with the help of the 1Sheeld application. The resultant yellow color is then transmitted to the 1Sheeld, which converts it into a digital response and finally provides the output by turning on the "yellow LED" (Fig. 10). This implies the absence of the target, *i.e.*, the specific toxic anion $CN^-$ in the unknown sample specimen. In the next phase, when low concentration and high concentration $CN^-$ were added into **DNMH** solution, vivid chromogenic changes from yellow to orangish red and intense red were observed, respectively. This concentration-dependent distinct colorimetric change is also evident from Fig. 9 (inset). The vial containing $CN^-$ solution is then placed inside the circular sample holder of the box and the camera takes the image. The transition in color was readily detected by the color sensor/detector application and was conveyed to the equipped 1Sheeld, thereby converting the chemical outcome into a digital one. Ultimately, the response was observed by turning on the "green LED" when low concentration of $CN^-$ was present (Fig. 11) and the "red LED" when high concentration of $CN^-$ was present (Fig. 12). The methodology provides a precise perception regarding the semi-quantitative detection of $CN^-$ in the unknown suspected sample specimen (Video S1†).

Table S17† describes a comparative table of $CN^-$ detecting probes, which showcases the standout advantages of **DNMH** in

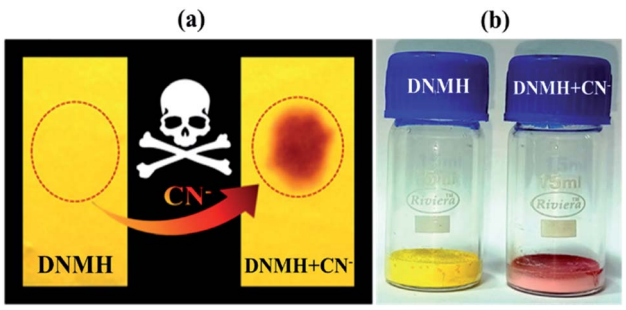


Fig. 8 Chromogenic changes of **DNMH** in the solid state: (a) chromatographic strips and (b) silica gel upon addition of $CN^-$ ions; **DNMH**, DNMH+$CN^-$.

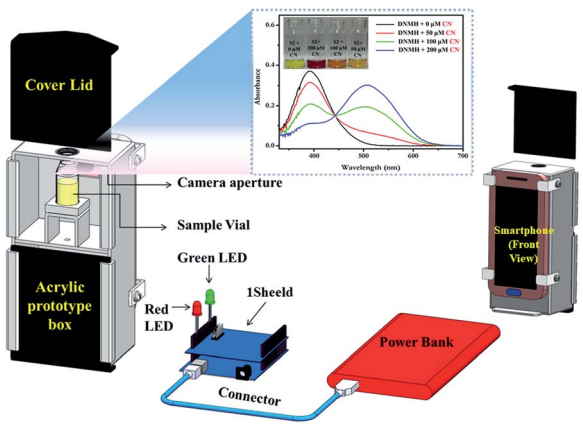


Fig. 9 AutoCAD diagram (rear view) representing an overview of the smartphone-based colorimetric prototype sensor [inset: UV-vis spectra of **DNMH** with varying $CN^-$ concentration].

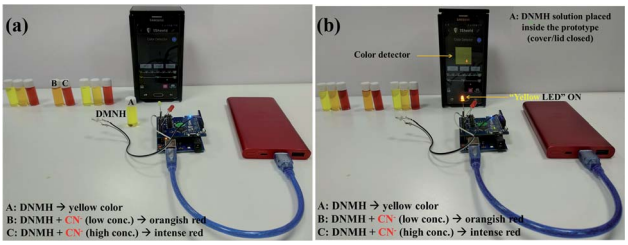


Fig. 10 (a) The smartphone-based prototype displaying (A) **DNMH** (yellow color) and (b) the prototype with the "yellow LED" ON: only **DNMH** sample solution is present.

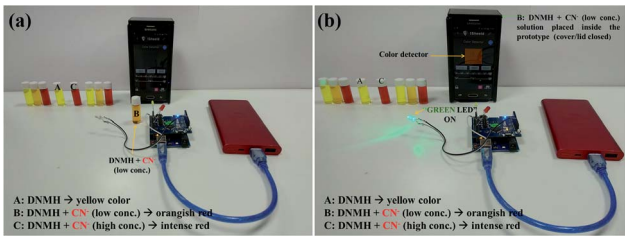


Fig. 11 (a) Prototype displaying (B) **DNMH**+$CN^-$ (low conc.) (orangish color) and (b) prototype with "green LED" ON: **DNMH**+$CN^-$ (low conc.) sample solution is analysed.

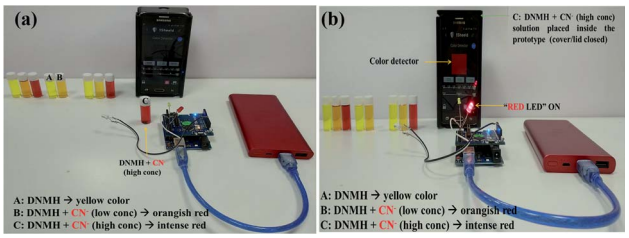


Fig. 12 (a) Prototype displaying (C) **DNMH**+$CN^-$ (high conc.) (intense red color): presence of high conc. of $CN^-$; (b) prototype with "red LED" ON: **DNMH**+$CN^-$ (high conc.) sample solution.

terms of detection limit, application in molecular logic circuitry, electrochemical detection and most significantly, its implementation in the smartphone-based colorimetric sensory prototype that makes the present work one of its kind and unprecedented among its congener of $CN^-$ sensors.

## Conclusions

In a nutshell, the present work reports a straightforward, cost-effective and rapid responsive naphthalene–hydrazine-functionalized Schiff base organic chemosensor (SOC) for the expeditious chromogenic detection of toxic analytes like $CN^-$. It induces a discernible "naked-eye" yellow to red colorimetric change in the presence of $CN^-$ with a substantially low detection threshold, a high value of association constant and excellent photostability. The recognition event has been rationalized through a "soft chemistry"-mediated change in the weak supramolecular non-covalent H-bonding interaction between the –NH proton of the chemosensor and the guest $CN^-$ in unison with an interesting additional blend in its feature of the recognition of highly toxic $Cd^{2+}$. Based on the relay recognition event with the ditopic ions $CN^-$ and $Cd^{2+}$, the reversibility of the chemosensing event by miniaturization with molecular electronics was executed following the logic circuitry algorithm. The experimental findings are also finely corroborated with the theoretical outcomes (DFT, TDDFT and FIs). The quick antibacterial response property of the SOC towards both Gram-positive (*Bt*) and Gram-negative bacteria (*E. coli*) has also been well established. Interestingly, the optical recognition phenomenon was furthermore amplified from a real-world perspective by developing "easy to prepare" chromatographic strips and a silica gel-based assay. Apart from this, a customized smartphone-assisted colorimetric sensory prototype was fabricated, demonstrating phenomenal efficiency in line with the economic and semi-quantitative point-of-use monitoring of perilous $CN^-$ in cyanide-intoxicated sample specimens. Therefore, the unique approaches as presented in the work including solution-state sensing and paper and silica gel-based solid-phase recognition along with the high-performance smartphone-assisted prototype demonstrates the present work to be a proof-of-concept next-generation solution towards the ultrasensitive monitoring of $CN^-$ like noxious analytes in the realm of supramolecular sensors.

## Conflicts of interest

There are no conflicts to declare.

## Acknowledgements

Financial support from the Council of Scientific & Industrial Research (CSIR), Govt. of India, (Ref. No. 33/2018/MD-FTT&FTC & Project No. MLP-223712) and Dept. of Science and Technology and Biotechnology (DSTBT), Govt. of West-Bengal [Ref No: 278(Sanc.)/ST/P/S&T/6G-35/2017 & Project No. GAP-222212] is hereby acknowledged. SP gratefully acknowledges DST INSPIRE for her fellowship [IF160302]. The authors are thankful to Mr Partha Mitra, IACS, Kolkata, Manilal Murmu, Research Scholar, CSIR-CMERI, Mr Subhasis Biswas and Mr Arabinda Sarkar, CSIR-CMERI, for their support.

## Notes and references

1 M. Cherbuin, F. Zelder and W. Karlen, *Analyst*, 2019, **144**, 130–136.
2 M. Xiao, Z. Liu, N. Xu, L. Jiang, M. Yang and C. Yi, *ACS Sens.*, 2020, **5**, 870–878.
3 S. Sajed, F. Arefi, M. Kolahdouz and A. Sadeghi, *Sens. Actuators, B*, 2019, **298**, 126942.
4 M. Islam, A. Hameed, K. Ayub, M. M. Naseer, J. Hussain, R. D. Alharthy, A. Asari, R. Ludwig, M. al. Rashida and Z. Shafiq, *ChemistrySelect*, 2018, **3**, 7633–7642.

5 M. Ishtiaq, I. Munir, M. Rashida, Maria, K. Ayub, J. Iqbal, R. Ludwig, K. M. Khan, S. A. Ali and A. Hameed, *RSC Adv.*, 2016, **6**, 64009–64018.
6 N. Iqbal, S. A. Ali, I. Munir, S. Khan, K. Ayub, M. Rashida, M. Islam, Z. Shafiq, R. Ludwig and A. Hameed, *RSC Adv.*, 2018, **8**, 1993–2003.
7 I. O. Isaac, I. Munir, M. Rashida, S. A. Ali, Z. Shafiq, M. Islam, R. Ludwig, K. Ayub, K. M. Khan and A. Hameed, *R. Soc. Open Sci.*, 2018, **5**, 180646.
8 V. Amendola, L. Fabbrizzi and L. Mosca, *Chem. Soc. Rev.*, 2010, **39**, 3889–3915.
9 H. J. Jang, J. H. Kang, M. Lee, M. H. Lim and C. Kim, *Ind. Eng. Chem. Res.*, 2018, **57**, 54–62.
10 G. Men, W. Han, C. Chen, C. Liang and S. Jiang, *Analyst*, 2019, **144**, 2226–2230.
11 F. Wang, L. Wang, X. Chen and J. Yoon, *Chem. Soc. Rev.*, 2014, **43**, 4312–4324.
12 M. T. Gabr and F. C. Pigge, *Dalton Trans.*, 2018, **47**, 2079–2085.
13 R. R. Dash, A. Gaur and C. Balomajumder, *J. Hazard. Mater.*, 2009, **163**, 1–11.
14 A. Tigrerosa, J. C. Castilloa and J. Portillaa, *Talanta*, 2020, **215**, 120905.
15 *Guidelines for Drinking Water Quality*, ed. M. Sheffer, World Health Organization, Geneva, 1996.
16 N. B. H. Anh and M. Sharp, *Anal. Chim. Acta*, 2000, **405**, 145–152.
17 S. Dadfarnia, M. A. Haji Shabani, F. Tamadon and M. Rezaei, *Microchim. Acta*, 2007, **158**, 159–163.
18 O. Destanoğlu, G. G. Yilmaz and R. Apak, *J. Liq. Chromatogr. Relat. Technol.*, 2015, **38**, 1537–1545.
19 H. Fang, C. Wang, Y. Chen, Z. Chen, S. Yao, S. Yang, L. Dong, Z. Guo and W. He, *Inorg. Chem. Front.*, 2021, **8**, 3402–3410.
20 T. Samanta, N. Das and R. Shunmugam, *ACS Sustainable Chem. Eng.*, 2021, **9**(30), 10176–10183.
21 L. A. Greenawald, G. R. Boss, J. L. Snyder, A. Reeder and S. Bell, *ACS Sens.*, 2017, **2**(10), 1458–1466.
22 Shaily, A. Kumar and N. Ahmed, *Ind. Eng. Chem. Res.*, 2017, **56**, 6358–6368.
23 R. Kaushik, A. Ghosh, A. Singh, P. Gupta, A. Mittal and A. D. Jose, *ACS Sens.*, 2016, **1**(10), 1265–1271.
24 P. Kumar, V. Kumar and R. Gupta, *Dalton Trans.*, 2020, **49**, 9544–9555.
25 P. Ghosh, A. R. Chowdhury, M. Corbella, A. Bhaumik, P. Mitra, S. M. Mobin, A. Mukherjee, S. Basu and P. Banerjee, *Dalton Trans.*, 2014, **43**, 13500–13508.
26 P. Ghosh, B. G. Roy, S. K. Mukhopadhyay and P. Banerjee, *RSC Adv.*, 2015, **5**, 27387–27392.
27 A. R. Chowdhury, P. Ghosh, B. G. Roy, S. K. Mukhopadhyay, P. Mitra and P. Banerjee, *RSC Adv.*, 2015, **5**, 62017–62023.
28 S. Paul, P. Ghosh, S. Bhuyan, S. K. Mukhopadhyay and P. Banerjee, *Dalton Trans.*, 2018, **47**, 1082–1091.
29 N. R. Pandit, S. Bej, A. Mondal, M. Ghosh, G. E. Kostakis, A. K. Powell, P. Banerjee and B. Biswas, *Dalton Trans.*, 2020, **49**, 13090–13099.
30 S. Bej, R. Das, H. Hirani and P. Banerjee, *Inorg. Chem.*, 2020, **59**(7), 4366–4376.
31 S. Paul and P. Banerjee, *Sens. Actuators, B*, 2021, **329**, 129172.
32 A. Mondal, S. Nag and P. Banerjee, *Dalton Trans.*, 2021, **50**, 429–451.
33 (*a*) U. Mondal, S. Bej, A. Hazra, S. Mandal, T. K. Pal and P. Banerjee, *Dalton Trans.*, 2022, **501**, 2083–2093; (*b*) A. Hazra, U. Mondal, S. Mandal and P. Banerjee, *Dalton Trans.*, 2021, **50**, 8657–8670; (*c*) D. Dey, A. Mondal, S. Nag, U. Mondal and H. Hirani, *New J. Chem*, 2021, **45**, 5156–5175.
34 R. Das, S. Bej, D. Ghosh, N. C. Murmu, H. Hirani and P. Banerjee, *Sens. Actuators, B*, 2021, **341**, 129925.
35 S. Bej, S. Mandal, A. Mondal, T. K. Pal and P. Banerjee, *ACS Appl. Mater. Interfaces*, 2021, **13**(21), 25153–25163.
36 (*a*) B. Delley, *J. Chem. Phys*, 1990, **92**, 508–517; (*b*) BIOVIA, Dassault systems, *Material Studio (Version 17.1.0.48)*, Dassault Systems, San Diego, 2017; (*c*) S. Mandal, M. Murmu, S. Sengupta, R. Baranwal, A. Hazra, H. Hirani and P. Banerjee, *J. Adhes. Sci. Technol*, 2022, 1–27.
37 S. C. Zimmerman, M. Mrksich and M. Baloga, *J. Am. Chem. Soc.*, 1989, **111**, 8528–8530.
38 B. H. Shankar, D. T. Jayaram and D. Ramaiah, *Chem.–Asian J.*, 2014, **9**, 1636–1642.
39 J. Ling, B. Daly, V. A. D. Silverson and A. P. de. Silva, *Chem. Commun.*, 2015, **51**, 8403–8409.
40 V. Kumar, M. P. Kaushik, A. K. Srivastava, A. Pratap, V. Thiruvenkatam and T. N. G. Row, *Anal. Chim. Acta*, 2010, **663**, 77–84.
41 S. Paul, S. Bhuyan, S. K. Mukhopadhyay, N. C. Murmu and P. Banerjee, *ACS Sustainable Chem. Eng.*, 2019, **7**(16), 13687–13697.
42 A. A. E. Bindary, N. Hassan and M. A. El. Afify, *J. Mol. Liq.*, 2017, **242**, 213–228.
43 R. R. Contreras, P. Fuenteal, M. Galvan and P. Perez, *Chem. Phys. Lett.*, 1999, **304**, 405–413.
44 A. Incel, O. Akin, A. Cagir, U. H. Yildiz and M. M. Demir, *Sens. Actuators, B*, 2017, **252**, 886–893.
45 R. Bhaskar and S. Sarveswari, *Inorg. Chem. Commun.*, 2019, **102**, 83–89.
46 S. Sajed, F. Arefi, M. Kolahdouz and M. A. Sadeghi, *Sens. Actuators, B*, 2019, **298**, 126942.